

# 1 Anisotropic Behaviour of Bituminous Mixtures in Road Pavement Structures

2 Quang Tuan Nguyen<sup>1</sup>, Nguyen Hoang Pham<sup>2</sup>, Hervé Di Benedetto<sup>3</sup>, Cédric Sauzéat<sup>3</sup>

3 (<sup>1</sup> University of Transport and Communications, Hanoi, Vietnam, quangtuan.nguyen@utc.edu.vn)

4 (<sup>2</sup> Thuyloi University, Hanoi, Vietnam, hoang.kcct@tlu.edu.vn)

5 (<sup>3</sup> LTDS (UMR CNRS 5513), University of Lyon/ENTPE, Vaulx-en-Velin, France,

6 herve.dibenedetto@entpe.fr, cedric.sauzeat@entpe.fr)

## 7 ABSTRACT

8 The compaction of bituminous mixture during the road pavement construction induces  
9 anisotropic properties. However, bituminous mixture is generally considered as isotropic. This  
10 paper presents the investigations on the anisotropic behaviour of bituminous mixture in road  
11 pavement structure. A pavement block (55×46×28cm) was sawn and extracted from a highway  
12 in France. Cylindrical specimens were cored and sawn from the middle layer of this block in  
13 three directions: longitudinal direction I, vertical direction II and transversal direction III.  
14 Complex tension/compression modulus tests were performed at ENTPE laboratory to investigate  
15 the anisotropic behaviour of bituminous mixture. These tests consist in measuring axial stress  
16 and radial strains when sinusoidal axial strain whose amplitude is lower than  $10^{-4}$  m/m was  
17 applied on the sample. Tests were performed on the 3 types of specimens (cored in directions I,  
18 II, III) at 9 temperatures and 6 frequencies. For each specimen, the complex modulus  $E^*$  and the  
19 complex Poisson's ratios  $\nu^*$  in two perpendicular diameter directions were measured. Thus, the  
20 three  $E^*$  ( $E^*_{I}$ ,  $E^*_{II}$  and  $E^*_{III}$ ) and the six  $\nu^*$  ( $\nu^*_{I-II}$ ,  $\nu^*_{I-III}$ ,  $\nu^*_{II-I}$ ,  $\nu^*_{II-III}$ ,  $\nu^*_{III-I}$ ,  $\nu^*_{III-II}$ ) could be obtained  
21 and investigated. The Time Temperature Superposition Principle was verified for both norm and  
22 phase angle of  $E^*$  and  $\nu^*$ . The anisotropic properties of material were studied by comparing the  
23 three  $E^*$  and six  $\nu^*$ . The obtained results reveal an anisotropic behaviour of bituminous mixture  
24 and the difference in  $E^*$  and  $\nu^*$  varied with the equivalent temperature-frequency. But rheological  
25 tensor was shown to be symmetric within the middle range of reduced frequency. The  
26 experimental results were then simulated using a 3D viscoelastic model. A unique normalised  
27 curve can be considered for  $E^*$  and  $\nu^*$  regardless of some dispersion for  $\nu^*$  values. Stability of the  
28 material behaviour was also investigated within the tested frequency-temperature range.

29 **Keywords:** anisotropy, bituminous mixtures, linear viscoelasticity, complex modulus,  
30 complex Poisson's ratio  
31

## 32 1. INTRODUCTION

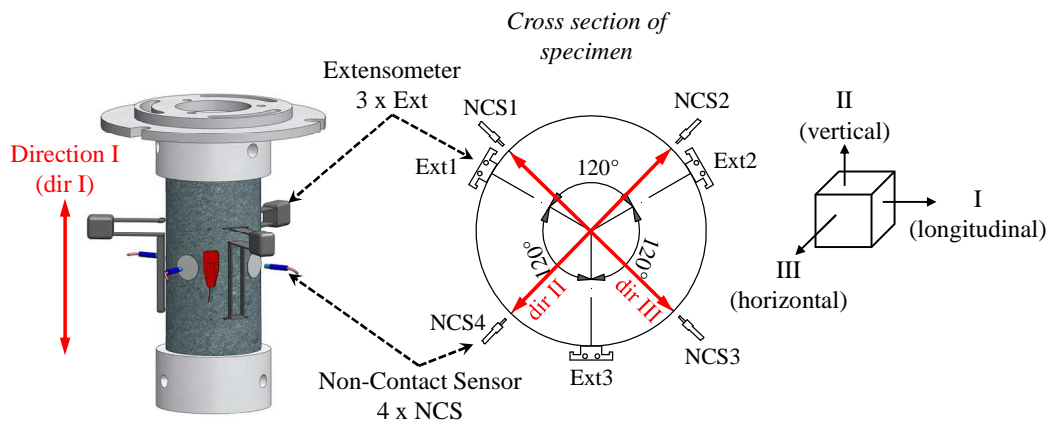
33 Bituminous mixture is generally considered as an isotropic material. In fact, the  
34 compaction during the road pavement construction can induce some anisotropic properties of this  
35 material. The anisotropic behaviour of bituminous mixture has been studied by very few authors  
36 [1-5]. This paper focuses on the anisotropic behaviour of field-compacted bituminous mixtures.  
37 The 3D tension-compression complex modulus tests were performed on cylindrical specimens  
38 that were cored and sawn from the bituminous mixture layer of a highway in France. The  
39 complex modulus  $E^*$  and the complex Poisson's ratios  $\nu^*$  were measured at different  
40 temperatures, frequencies and at small applied strain amplitudes ( $< 100 \mu\text{m/m}$ ). The anisotropic  
41 properties of material were studied by comparing the complex moduli  $E^*$  and the complex

1 Poisson's ratios  $\nu^*$  in different material directions. In addition, the Time Temperature  
 2 Superposition Principle (TTSP) [6-8] was verified for the tested bituminous mixture.  
 3

## 4 2. MATERIALS AND 3D COMPLEX MODULUS TESTS

5 A pavement block (55×46×28 cm) which comprises 3 bituminous mixture layers (28 cm  
 6 in total depth) was sawn and extracted from a highway in France. Cylindrical specimens (75 cm  
 7 in diameter and 140 cm high) were cored and sawn from the middle layer (11 cm in depth) of  
 8 this block in three directions: longitudinal direction (direction I), vertical direction (direction II)  
 9 and transversal direction (direction III).

10 Complex modulus tests were performed on three specimens BI, BII, BIII cored in three  
 11 directions I, II, III, respectively. For each specimen, the complex modulus  $E^*$  and the complex  
 12 Poisson's ratios  $\nu^*$  in two perpendicular diameter directions (see Figure 1) were measured at nine  
 13 temperatures (from -16°C to 40°C) and six frequencies (from 0.03 Hz to 10 Hz). Thus, the three  
 14  $E^*$  ( $E^*_I$ ,  $E^*_II$  and  $E^*_III$ ) and the six  $\nu^*$  ( $\nu^*_{I-II}$ ,  $\nu^*_{I-III}$ ,  $\nu^*_{II-I}$ ,  $\nu^*_{II-III}$ ,  $\nu^*_{III-I}$ ,  $\nu^*_{III-II}$ ) of tested bituminous  
 15 mixture could be obtained for a large range of temperature and frequency. The set up for  
 16 accurate measurements of axial and radial strains (Figure 1) has been developed at ENTPE for  
 17 many studies [9-11]. Due to the limit of the paper, details on the test equipment are not  
 18 presented.



19 **FIGURE 1 Measurement of axial strain, radial strains on specimen cored in direction I**  
 20  
 21

22 When the sinusoidal axial strain is applied in direction I, the sinusoidal evolution with  
 23 time of measured stress and strains is defined by Eqs.(1, 2, 3), where  $\phi_{E I}$  is the phase angle  
 24 between the strain in direction I ( $\epsilon_I$ ) and the stress in direction I ( $\sigma_I$ ).  $\phi_{v II-I}$ ,  $\phi_{v III-I}$  are the phase  
 25 angle between the strain in direction I ( $\epsilon_I$ ) and the strain in direction II, III ( $\epsilon_{II}$ ,  $\epsilon_{III}$ ), respectively.

$$26 \quad \epsilon_I(t) = \epsilon_{0I} \sin(\omega t) \quad (1)$$

$$27 \quad \sigma_I(t) = \sigma_{0I} \sin(\omega t + \phi_{E I}) \quad (2)$$

$$28 \quad \epsilon_i(t) = -\epsilon_{0i} \sin(\omega t + \phi_{v i-I}) \quad (i = II, III) \quad (3)$$

29 From Eqs.(1, 2, 3), the complex modulus in direction I ( $E^*_I$ ) and two complex Poisson's  
 30 ratios in direction II and III ( $\nu^*_{II-I}$ ,  $\nu^*_{III-I}$ ) can be given by Eqs.(4, 5), where  $j$  is the complex  
 31 number ( $j^2 = -1$ ).

$$E_I^* = \frac{\sigma_{0I}}{\varepsilon_{0I}} e^{j\phi_{E1}} = |E_I^*| e^{j\phi_{E1}} \quad (4)$$

$$v_{i-I}^* = \frac{\varepsilon_{0i}}{\varepsilon_{0I}} e^{j\phi_{v_{i-I}}} = |v_{i-I}^*| e^{j\phi_{v_{i-I}}} \quad (i = \text{II, III}) \quad (5)$$

The relation between stress and strain, expressed in principal axes I, II, III, is defined by Eq.(6), where  $\underline{\underline{M}}^*$  is the complex compliance tensor.

$$\underline{\underline{\varepsilon}}^* = \underline{\underline{M}}^* \underline{\underline{\sigma}}^* \quad \text{with} \quad \underline{\underline{M}}^* = \begin{pmatrix} \frac{1}{E_I^*} & -\frac{v_{I-II}^*}{E_{II}^*} & -\frac{v_{I-III}^*}{E_{III}^*} \\ -\frac{v_{II-I}^*}{E_I^*} & \frac{1}{E_{II}^*} & -\frac{v_{II-III}^*}{E_{III}^*} \\ -\frac{v_{III-I}^*}{E_I^*} & -\frac{v_{III-II}^*}{E_{II}^*} & \frac{1}{E_{III}^*} \end{pmatrix} \quad (6)$$

6

### 7 3. TEST RESULTS

8 Figures 2 and 3 present the measured complex modulus  $E^*$  of three tested specimens BI,  
 9 BII and BIII. Figure 2 shows the complex modulus in Cole-Cole diagram and Black diagram.  
 10 The master curves of norm and phase angle of complex modulus at the reference temperature  $T_R$   
 11 = 15°C were plotted in Figure 3. The results in Figures 2 and 3 indicated that complex modulus  
 12 in all three directions respects the TTSP. At low temperature (high frequency), the modulus of  
 13 BIII specimen is highest, followed by BI and BII specimens. At high temperature, the BI  
 14 specimen has a higher norm of complex modulus  $|E^*|$  than one of BII and BIII specimens. The  
 15 behaviour of tested bituminous mixture can be considered anisotropic. The 2S2P1D model was  
 16 used to simulate the linear viscoelastic behaviour of material in each direction. The readers can  
 17 find more details of this model in [12]. The simulation of  $E^*$  with 2S2P1D model is also  
 18 presented in Figures 2 and 3.

19

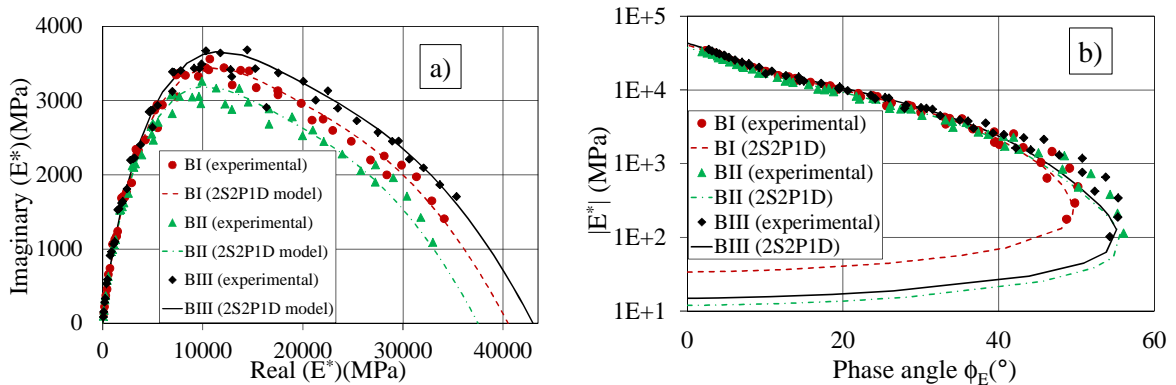


**FIGURE 2 Complex modulus in Cole-Cole diagram (a) and Black diagram (b)**

20  
 21  
 22

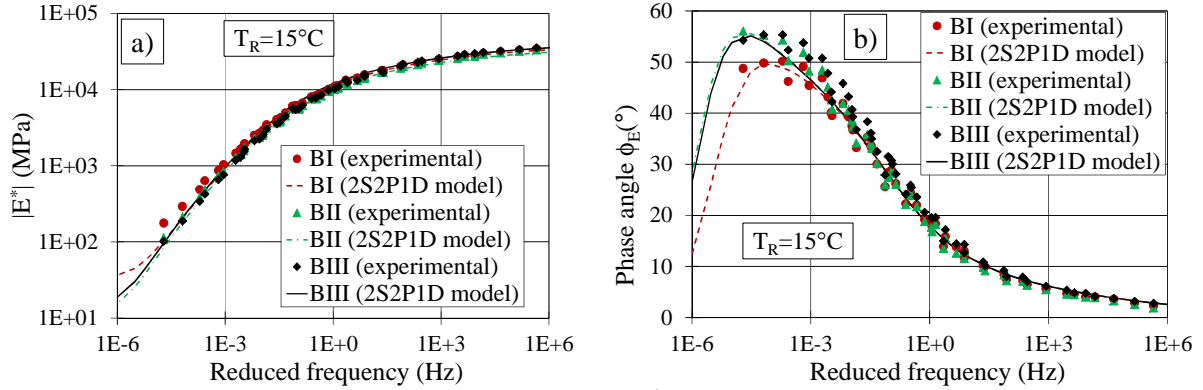


**FIGURE 3 Master curves of  $|E^*|$  (a) and  $\phi_E$  (b) at  $T_R = 15^\circ\text{C}$**

1  
2  
3  
4  
5  
6  
7  
8  
9  
10  
11  
12  
13

Figure 4 presents the master curves of all  $|v^*|$  (norm of complex Poisson's ratio) plotted at the reference temperature  $T_R = 15^\circ\text{C}$ . This result shows that the TTSP is verified and applicable in the 3D case. It can be seen that the value of  $|v_{\text{III-II}}^*|$  is highest on the whole tested range of reduced frequency. At low frequency, the value of  $|v_{\text{III-I}}^*|$  is smallest. At high frequency, the values of  $|v_{\text{I-II}}^*|$  and  $|v_{\text{I-III}}^*|$  are smallest. The good fitting of data for both  $E^*$  and  $v^*$  in Figures 2, 3, 4 confirms the good performance of 2S2P1D model. It should be underlined that the shift factors used to build the master curves of  $E^*$  and  $v^*$  of all three specimens are identical. In addition, the simulation by 2S2P1D model used the same viscous and temperature constants for all three specimens. These remarks are important when modelling the anisotropic behaviour of tested bituminous mixtures.

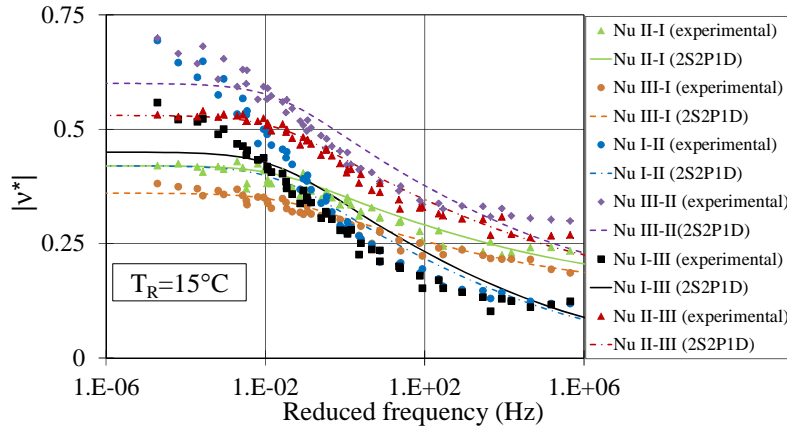


**FIGURE 4 Master curves of  $|v^*|$  at  $T_R = 15^\circ\text{C}$**

14  
15  
16  
17  
18  
19  
20  
21  
22  
23

The normalised complex modulus  $(E^* - E_{00})/(E_0 - E_{00})$  and normalised complex Poisson's ratio  $(v^* - v_{00})/(v_0 - v_{00})$  as a function of reduced frequency are presented in Figure 5.  $E_{00}$  and  $E_0$  ( $v_{00}$  and  $v_0$ ) are asymptotic values of the norm of complex modulus (the norm of complex Poisson's ratio) when the frequency tends towards 0 and infinity, respectively.  $E_{00}$ ,  $E_0$ ,  $v_{00}$  and  $v_0$  are determined by the simulation using the 2S2D1P model. The results in Figure 5 indicated that the normalised  $E^*$  and  $v^*$  curves of all three specimens are close regardless of some dispersion for normalised  $v^*$  values at high temperature/low frequency.

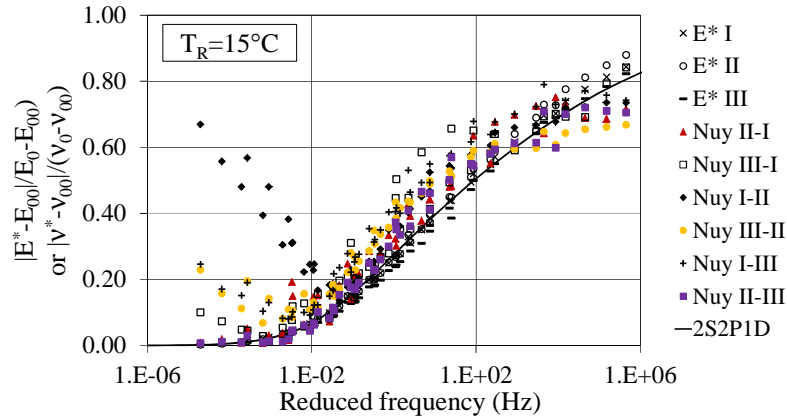


**FIGURE 5 Normalised  $E^*$  and normalised  $v^*$  as a function of reduced frequency**

The symmetry of compliance tensor  $\underline{M}^*$  (Eq.(6)) was verified and presented in Figure 6.

Each couple of  $|v^*/|E^*|$ , which corresponds symmetric terms of tensor  $\underline{M}^*$ , was compared together on the whole tested range of temperature and frequency. The results indicated that the compliance tensor can be considered as symmetric at middle values of reduced frequency (from 0.01 Hz to 10 Hz) at  $T_R = 15^\circ\text{C}$ . At high and low reduced frequency, the tensor is not symmetric.

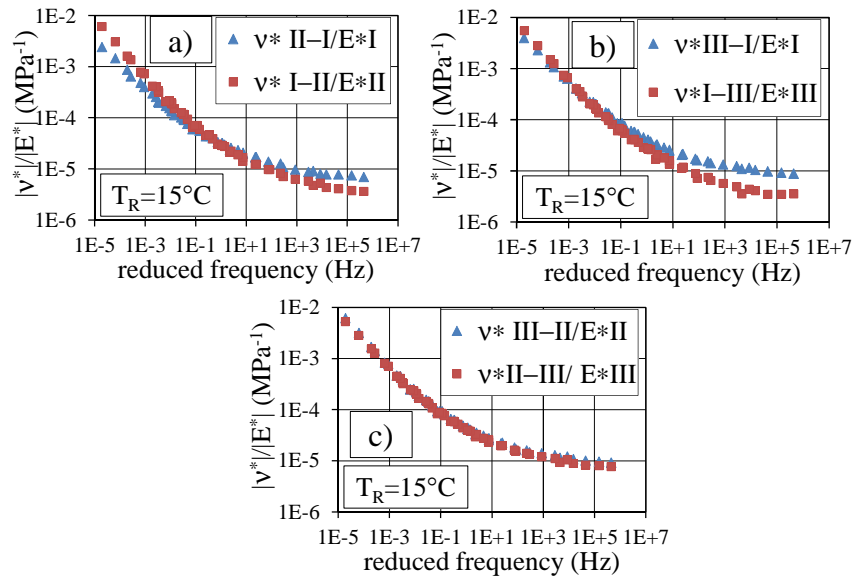


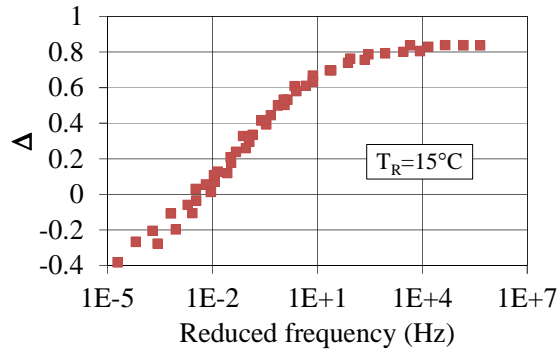
**FIGURE 6 Verification of symmetry of compliance tensor  $\underline{M}^*$**

In the linear elastic case, the necessary and sufficient condition giving the stability of behaviour from thermodynamics consideration is expressed by Eq.(7) [13].

$$\Delta = 1 - \nu_{I-II}\nu_{II-I} - \nu_{II-III}\nu_{III-II} - \nu_{III-I}\nu_{I-III} - 2\nu_{II-I}\nu_{III-II}\nu_{I-III} > 0 \quad (7)$$

Making analogy with linear elastic case, validity of Eq. (7) was checked on the whole frequency temperature range, for norm of the complex Poisson's ratios. The values of  $\Delta$  as a function of reduced frequency were plotted in Figure 7. The result shows that the condition given

1 by Eq. (7) is respected for the reduced frequency higher than 0.0033 Hz at  $T_R = 15^\circ\text{C}$ . At lower  
 2 reduced frequency, this condition is not respected. In fact, very high accuracy is needed to  
 3 measure Poisson's ratio  $\nu^*$  at high frequencies/low temperatures and low frequencies/high  
 4 temperatures. This remark should be considered when analysing the difference between  
 5 symmetric terms  $|\nu^*|/|E^*|$  at high and low reduced frequency (Figure 6) and the negative values of  
 6  $\Delta$  at very low reduced frequencies (Figure 7).



7  
 8 **FIGURE 7 Values of  $\Delta$  as a function of reduced frequency at  $T_R = 15^\circ\text{C}$**

9 **3. CONCLUSIONS**

10 This paper focuses on the linear viscoelastic (LVE) behaviour and the anisotropic  
 11 behaviour of bituminous mixture in road pavement structure. From the obtained results, the  
 12 following conclusions can be drawn:

- 13 • The Time Temperature Superposition Principle (TTSP) was verified for both norm and  
 14 phase angle of complex modulus  $E^*$  and complex Poisson's ratio  $\nu^*$ . The master curves of  
 15  $E^*$  and  $\nu^*$  of three specimens cored in three directions I, II, III were built using the same  
 16 shift factors.
- 17 • The 2S2P1D model shows a good simulation of 3D LVE behaviour of tested bituminous  
 18 mixture. The viscous constants of this model are identical for  $E^*$  and  $\nu^*$  of all three tested  
 19 specimens BI, BII, BIII (cored in direction I, II, III, respectively).
- 20 • From experimental results, the difference in  $E^*$  and  $\nu^*$  of specimens cored in different  
 21 directions was observed. This difference varied with the equivalent temperature-  
 22 frequency. The behaviour of specimens extracted from a highway in France can be  
 23 considered as anisotropic.
- 24 • The rheological tensor was shown to be symmetric within the middle range of reduced  
 25 frequency. At high and low reduced frequency, the symmetry was not observed but this  
 26 point needs to be further investigated.
- 27 • The normalised  $E^*$  and  $\nu^*$  curves of three specimens are close and can be considered as  
 28 identical if unavoidable dispersion for normalised  $\nu^*$  values at high temperature/low  
 29 frequency are considered.
- 30 • Stability of the material behaviour was verified within the tested frequency-temperature  
 31 range. The necessary and sufficient condition giving the stability of material behaviour is  
 32 respected for the middle and high reduced frequency ( $> 0.0033$  Hz at  $T_R = 15^\circ\text{C}$ ).

## 1 REFERENCES

- 2 [1] Motola Y. and Uzan J. Anisotropy of field-compacted asphalt concrete material,  
3 *Journal of Testing and Evaluation*, 35(1), pp. 103–105. 2007.
- 4 [2] Clec'h P., Sauzéat C., Di Benedetto H. Linear viscoelastic behavior and anisotropy of  
5 bituminous mixture compacted with a French wheel compactor, 2<sup>nd</sup> International GeoShanghai  
6 Conference, p. 13. 2010.
- 7 [3] Gajewski M. and Jemioło S. Orthotropic composite constitutive model of mineral  
8 asphalt mix reinforced with grid and its approximation with an isotropic model, *Road Materials*  
9 *and Pavement Design*, 15(3), pp. 521–538. 2014.
- 10 [4] Pham N.H., Sauzéat C., Di Benedetto H., Gonzalez-Leon J.A., Barreto G., Nicolai A.,  
11 Jakubowski M. Reclaimed Asphalt Pavement and additives influence on 3D linear behaviour of  
12 warm mix asphalts, *Road Materials and Pavement Design*, 16(3), pp. 569–591 . 2015.
- 13 [5] Di Benedetto H., Sauzéat C., Clec'h P., Anisotropy of bituminous mixture in the  
14 linear viscoelastic domain, *Mechanics of Time-Dependent Materials*, 20(3), pp. 281–297. 2016.
- 15 [6] Perraton D., H. Di Benedetto, C. Sauzéat, B. Hofko, A. Graziani, Q.T. Nguyen, S.  
16 Pouget, Lily D. Poulidakos, N. Tapsoba, J. Grenfell, 3Dim experimental investigation of linear  
17 viscoelastic properties of bituminous mixtures, *Materials and Structures*, 49(11), pp. 4813-4829.  
18 2016.
- 19 [7] Nguyen Q.T., Di Benedetto H., Sauzéat C., Tapsoba N. Time Temperature  
20 Superposition Principle Validation for Bituminous Mixes in the Linear and Nonlinear Domains,  
21 *Journal of Materials in Civil Engineering*, 25 (9), pp. 1181–1188. 2013.
- 22 [8] Nguyen Q.T., Di Benedetto H., Sauzéat C. Linear and nonlinear viscoelastic  
23 behaviour of bituminous mixtures, *Materials and Structures*, 48(7), pp. 2339-2351. 2015
- 24 [9] Nguyen Q.T., Di Benedetto H., Sauzéat C. Effect of fatigue cyclic loading on linear  
25 viscoelastic properties of bituminous mixtures, *Journal of Materials in Civil Engineering*, 27(8).  
26 2015.
- 27 [10] Pham NH, Sauzéat C, Di Benedetto H, Gonzalez-Leon JA, Barreto G, Nicolai A,  
28 Jakubowski M. Analysis and modeling of 3D complex modulus tests on hot and warm  
29 bituminous mixtures. *Mechanics of Time Dependent Materials*, 19(2), pp. 167-186. 2015.
- 30 [11] Nguyen Q.T., Di Benedetto H., Sauzéat C, Nguyen M.L., Hoang T.T.N. 3D complex  
31 modulus tests on bituminous mixture with sinusoidal loadings in tension and/or compression,  
32 *Materials and Structures*, 50(1), pp. 8. 2017.
- 33 [12] Di Benedetto H., Delaporte B., Sauzéat C. Three-dimensional linear behavior of  
34 bituminous materials: experiments and modelling, *International Journal of Geomechanics*, 7(2),  
35 pp. 149–157. 2007.
- 36 [13] Chevalier Y., Comportement élastique et viscoélastique des composites, *Techniques*  
37 *de l'ingénieur A7750* [in French]. 1988.